Resonant absorption of electromagnetic waves by an induced inhomogeneity in a liquid metamaterial

Alexander Zharov, Vanessa Fierro, Alain Celzard

Resonant absorption of electromagnetic waves by an induced inhomogeneity in a liquid metamaterial

Alexander Zharov*
Université de Lorraine, CNRS, IJL,F-88000 Epinal, France and
Institute for Physics of Microstructures, Russian Academy of Sciences, Nizhny Novgorod 603950, Russia

Vanessa Fierro and Alain Celzard†
Université de Lorraine, CNRS, IJL,F-88000 Epinal, France

In this study, we consider the scattering of a plane electromagnetic wave on a cylindrically inhomogeneous distribution of meta-atoms in a liquid metamaterial. The distribution inhomogeneity appears naturally as a result of the application of an electric potential to an electrode immersed in the liquid metamaterial, which leads to the appearance of inhomogeneity in the effective permittivity of such a medium. Consequently, in the considered type of metamaterial, the concentration-dependent effective permittivity can become negative in some region of space. In the vicinity of the interface between positive and negative permittivity, the behavior of the electromagnetic wave becomes singular, giving rise to effects such as resonant absorption, resonant scattering, and shielding of the central region.These effects can be controlled in real time by changing the applied electric potential and thus rearranging the liquid metamaterial.

I. INTRODUCTION

Since the first studies [1, 2], the primary motivation for developing and manufacturing metamaterials (MMs) has been the ability to control electromagnetic fields at micro- and nanoscale. In general, the peculiar electromagnetic properties of MMs are conditioned by the special design of their structural elements, called meta-atoms. During the years of MM research, different types of MMs have been studied and fabricated, such as linear and non-linear negative-index (or left-handed) MMs [3–8], tunable non-linear, elastic, and disordered MMs [9–12], plasmonic MMs [13, 14], and so-called artificial hyperbolic media [15–17]. Depending on the meta-atom design, these materials can exhibit their distinctive properties at frequencies ranging from microwaves to optical. As a result, MMs have found applications in invisibility cloaking [18, 19], superlensing [20, 21], transformation optics [22, 23], and enhancement of chirality and optical activity [24, 25].

Amongst others, liquid MMs [26] are distinguished by their high tunability and reconfigurability. In particular, nanocluster plasmonic negative index metafluids [27, 28], colloidal MMs [29], hybrid liquid crystal-based colloids [30], and liquid metacrystals [31–34] have been studied theoretically and experimentally. The simplest liquid MM can be imagined as an array of identical isotropic particles suspended in a viscous liquid. If the size of the particles is well below the wavelength, then such a suspension can be treated as an effective continuous medium with effective macroscopic permittivity and permeability. These macroscopic effective parameters, however, are defined by the microscopic properties of each meta-atom. Even the most obvious meta-atom design, a homogeneous sphere, can lead to non-trivial behavior. For instance, the electrical polarizability of metallic particles can become negative above the plasmon resonance, while in dielectric particles, either the magnetic or the electrical polarizability can be negative due to Mie resonances. As a result, when the meta-atom concentration is sufficient, the effective permittivity (or permeability) can become negative. Moreover, by using the special meta-atom design, negative permittivity and permeability can be achieved simultaneously [35].

A particular case of interest is the behavior of an electromagnetic wave in an MM with continuously varied permittivity, especially near the zero-index transition point, *i.e.*, the point where the refractive index crosses zero. MMs with linear index transition have been studied in [12, 36, 37]. Notably, anomalous field enhancement and resonant absorption in the vicinity of the transition point were predicted. Similar effects are observed in inhomogeneous plasmas with the permittivity changes sign [38].

In this study, we analyze the scattering of a plane electromagnetic wave on a cylindrically symmetric inhomogeneity of a liquid MM. The inhomogeneity appears naturally as a result of the electrophoretic pull of meta-atoms in the region of stronger electric field, which is controlled by applying an electric potential to a metallic electrode immersed in the MM. The meta-atoms are treated as spherical particles made of a Drude material, thus having a negative polarizability in a certain frequency range. Therefore, in the region of the highest meta-atom concentration, the effective permittivity can become negative, which leads to a singular behavior of the electromagnetic field near the transition from positive to negative permittivity. This gives rise to effects such as resonant absorption, resonant scattering, and shielding of the central region.

II. MODEL DESCRIPTION

As a model problem, we consider a transparent container filled with a liquid MM with a cylindrical electrode immersed in it, as shown in Fig. 1. We assume that the size of the container is much larger than any other scale in the problem. In particular, in what follows, we will consider the scattering of a plane electromagnetic wave on the metamaterial inhomogeneity induced by the immersed electrode, and we will not take into account the influence of the outer boundary of the container. In other words, we will neglect the scattering on the

external surfaces of the container and focus solely on its inner part.

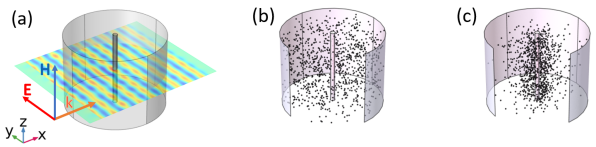

FIG. 1. (a) Schematic picture of the considered system. The system is illuminated by a plane electromagnetic wave. The outer boundary of the container is schematically represented by the external cylinder. However, it is assumed that it has no impact on the electromagnetic wave propagation. (b) Meta-atom distribution without applied voltage. (c) Meta-atom distribution with applied voltage.

The MM is regarded as a suspension of subwavelength spherical particles, the meta-atoms, which possess isotropic negative polarizability in a certain frequency range. The meta-atoms are considered non-interacting, *i.e.*, we assume that they do not tend to agglomerate and we neglect the dipole-dipole interaction between them. As long as the conditions of the effective medium approximation are fulfilled, the exact nature of the meta-atoms is not relevant here; for example, the meta-atoms can be metallic or dielectric spheres. In the first case, the negative polarizability can be achieved at frequencies above the plasmon resonance, while in the second case the negative polarizability can be caused by Mie resonances. We assume that the meta-atom size is much smaller than the wavelength λ, and the concentration of meta-atoms n satisfies the condition $n^{1/3}\lambda \gg 1$, *i.e.*, the number of particles in a wavelength scale is much greater than one. Thus, the MM can be treated as an effective continuous medium with an effective relative permittivity ε_{eff}. In general, ε_{eff} can be calculated as follows [39]:

$$\varepsilon_{\text{eff}} = \varepsilon_h - \frac{\frac{3\nu\varepsilon_h}{2q^3}\left[\sum_{j=1}^{N} i(2j+1)(a_j+b_j)\right]}{1+\frac{\nu}{2q^3}\left[\sum_{j=1}^{N} i(2j+1)(a_j+b_j)\right]} \tag{1}$$

where ε_h is the relative permittivity of the host medium, $q = 2\pi\sqrt{\varepsilon_h}\lambda^{-1}$ is the size parameter of a meta-atom, $\nu = nV_0$ is the volume fraction of meta-atoms; n is the concentration of meta-atoms and V_0 is the volume of a single meta-atom, i is the imaginary unit, a_j and b_j are the Mie coefficients of j^{th} order, and N is the cutoff number. However, in the present work, we will restrict ourselves to considering a particular case of meta-atoms made of a Drude material near the plasmon resonance. In this case, the electric dipole Mie coefficient is dominant over the other multipoles, *i.e.*, $a_1 \gg b_1, a_2 \ldots$ Therefore, Eq. (1) can be simplified to the well-known Maxwell Garnett approximation:

$$\varepsilon_{\text{eff}} = \varepsilon_h\left(1+3\nu\frac{\varepsilon_{MA}-\varepsilon_h}{\varepsilon_{MA}(1-\nu)+\varepsilon_h(2+\nu)}\right), \tag{2}$$

where ε_{MA} is the relative permittivity of the meta-atoms.

When no voltage is applied to the immersed electrode, *i.e.*, when the potential of the electrode is equal to that which is remote from the electrode and the electric field is zero, the meta-atoms in thermal equilibrium are distributed uniformly in space. This corresponds to a uniform concentration and, consequently, to a homogeneous effective permittivity. On the other hand, the non-zero potential u applied to the immersed electrode induces an electric charge in it and, therefore, gives rise to the cylindrically symmetric static electric field in the vicinity of the electrode, which can be written as:

$$\mathbf{E}(\rho) = \rho_{\mathbf{0}}\frac{ql^{-1}}{2\pi\varepsilon_0\varepsilon(\rho)}\frac{1}{\rho} = \rho_{\mathbf{0}}\frac{u}{\log(l/r_i)\varepsilon(\rho)}\frac{1}{\rho}, \tag{3}$$

where $\mathbf{E}(\rho)$ is the electric field, $\rho_{\mathbf{0}}$ is the unit vector in the radial direction in the cylindrical coordinate system (ρ,ϕ,z), ρ is the corresponding radial coordinate, q is the electric charge of the electrode, ε_0 is the permittivity of vacuum, $\varepsilon(\rho)$ is the static relative permittivity of the medium at the coordinate ρ, u is the applied potential measured with respect to zero potential at infinity, and l and r_i are the length and the radius of the electrode. The electric charge q induced by the voltage u was found to take the form $q = Cu \approx 2\pi\varepsilon_0 lu/\log(l/r_i)$, where C is the capacitance of an isolated conductive cylinder taken in the limit of an infinite length-to-radius ratio [40]. Equation (3) is valid for $\rho \ll l$, *i.e.*, when the electrode can be treated locally as an infinite cylinder. Thus, the problem will be further treated as two-dimensional in the plane perpendicular to the cylinder axis. The electric field induces dipole moments in meta-atoms, which, in turn, interact with the electric field, producing the electrophoretic force $\mathbf{F}_{EF}$:

$$\mathbf{F}_{EF} = (\mathbf{p}\nabla)\mathbf{E} = \rho_{\mathbf{0}}\alpha_0 E\frac{\partial E}{\partial\rho}, \tag{4}$$

where $\mathbf{p}$ is the dipole moment of a meta-atom, α_0 is the polarizability of a meta-atom, and E is the magnitude of the electric field at the meta-atom position. Substituting Eq. (3) in Eq. (4), we obtain:

$$\mathbf{F}_{EF} = -\rho_{\mathbf{0}}\alpha_0\left(\frac{u}{\log(l/r_i)\varepsilon(\rho)}\right)^2\frac{1}{\rho^3}. \tag{5}$$

Evidently, the electrophoretic force attracts the meta-atoms to the central electrode, making their concentration inhomogeneous. It should be noted that the force does not depend on the sign of the potential difference or the direction of the electric field vector. The particles are always attracted to the region where the field is the highest. The equilibrium distribution of meta-atoms can be found by applying the Gibbs formula:

$$f(\rho) = A_0\exp\left(-\frac{U(\rho)}{k_BT}\right), \tag{6}$$

where $f(\rho)$ is the meta-atom distribution function, $U(\rho)$ is the potential energy of a meta-atom in the field of the electrophoretic force given by Eq. (5), k_B is the Boltzmann constant, and T is the temperature. The normalization constant A_0 is defined from the normalization condition:

$$\iiint_V f(\rho)\,d^3\mathbf{r} = N, \tag{7}$$

where V is the volume of the container and N is the total number of meta-atoms. With this normalization, the distribution function readily provides the local concentration $n(\rho)$ as a function of ρ: $n(\rho) = f(\rho)$. The potential energy $U(\rho)$ can be calculated as follows:

$$U(\rho) = -\mathbf{pE} = -\alpha_0 \left(\frac{u}{\log(l/r_i)\varepsilon(\rho)} \right)^2 \frac{1}{\rho^2}. \quad (8)$$

Thus, the distribution function and, therefore, the radial dependence of the meta-atom concentration, takes the form:

$$f(\rho) = n(\rho) = A_0 \exp\left(\frac{\alpha_0}{k_B T} \left(\frac{u}{\log(l/r_i)\varepsilon(\rho)} \right)^2 \frac{1}{\rho^2} \right). \quad (9)$$

The evident complication arises from the fact that the local relative dielectric permittivity $\varepsilon(\rho)$ is itself affected by the redistribution of meta-atoms governed by Eq. (9). Indeed, the local permittivity in the considered statement of the problem is simply the effective relative permittivity ε_{eff} defined by Eq. (2), which contains the volume fraction ν, which, in turn, is specified by the local meta-atom concentration. Naively, the local effective relative permittivity could be approximated by its unperturbed value. In such a case, the applicability conditions have to be supplemented by an additional restriction on the maximum concentration, limiting the deviation of the effective permittivity from its unperturbed value due to the change in the meta-atom concentration. On the other hand, this restriction may contradict the need to obtain a negative effective permittivity at high frequency. Indeed, due to the frequency dispersion, for some types of meta-atoms, it is possible that the perturbation of the static permittivity is small, while its high-frequency variation is not. However, for meta-atoms made of a material with Drude permittivity, which we will explicitly consider in this paper, the meta-atom contribution to the effective permittivity at zero frequency is never less than that at any finite frequency. Therefore, the meta-atom distribution was found self-consistently using numerical methods.

It should be noted that the derived distribution is only valid when the concentration does not reach the close-packing values. Otherwise, an interparticle interaction term must be introduced into the energy, and a more complicated problem has to be solved to derive the distribution.

In the considerations above, the gravitation effects on the redistribution of meta-atoms have been neglected. To find the applicability conditions of such an approximation, the influences of gravity and electric field on the meta-atoms have to be compared. This can be done by comparing the potential energy given by Eq. (8) with the gravitational potential energy $U_G = m_{MA} g l$, where m_{MA} is the mass of a meta-atom, $g = 9.8$ m/s^2 is the free-fall acceleration, and l, being the length of the electrode, represents the characteristic scale of the system. The straightforward estimation shows that if we limit the voltage to a maximum of 600 V, the maximum radius of the electrode when the gravitation can be neglected is $r_i \approx 100$ μm.

Distribution (9) may be rewritten in a more convenient way as

$$f(\rho) = n(\rho) = A_0 \exp\left(\left(\frac{u}{u_0} \right)^2 \frac{1}{(\varepsilon_{\text{eff}}(\rho)/\varepsilon_h)^2} \frac{1}{(\rho/r_i)^2} \right), \quad (10)$$

where $u_0^2 = k_B T r_i^2 \alpha_0^{-1} \varepsilon_h^2 \log^2(l/r_i)$ is some characteristic voltage of the system. By definition, it determines the voltage at which the electrophoretic force predominates over the thermal fluctuations. For instance, in a system at room temperature, 300 K, with the electrode radius of 1 μm and 10-nm-radius meta-atoms, the characteristic voltage is $u_0 \approx 39.5$ V. On the other hand, the form of Eq. (10) determines the scaling properties of the meta-atom distribution. Indeed, as far as the ratio u/u_0 and the host permittivity ε_h are fixed, the meta-atom distribution over the dimensionless coordinate ρ/r_i remains the same, no matter what the particular parameters of the system are.

The radial dependence of the effective permittivity $\varepsilon_{\text{eff}}(\rho)$ was obtained as a self-consistent solution of Eqs. (10) and (2) with the normalization condition Eq. (7). The possible effective permittivity profiles at different voltages are shown in Fig. 2. For definitiveness, we supposed that the meta-atoms are spheres made of a Drude material whose permittivity is given by $\varepsilon_{MA}(\omega) = 1 - \omega_p^2/(\omega^2 + i\gamma\omega)$, where ω is the electromagnetic wave frequency, ω_p is the plasma frequency, and γ is the damping factor, which defines the losses in the meta-atoms material. We will focus on the cases where the real part of the permittivity changes sign and becomes negative at some point. Evidently, the region with negative real part of the effective permittivity appears when the voltage reaches some threshold value, which is determined by the parameters of the system.

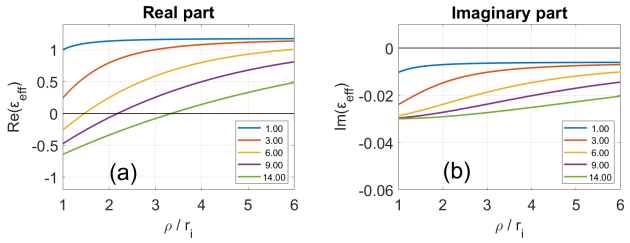

FIG. 2. Real (a) and imaginary (b) parts of the possible effective permittivity dependences on the normalized distance from the cylinder center for different dimensionless voltages, $u/u_0 = 1$, 3, 6, 9, and 14. The calculations were made for the host permittivity $\varepsilon_h = 1.4$. The meta-atom material was meant to have Drude permittivity; the frequency was set to $0.7\omega_p$. The unperturbed meta-atom volume fraction was set to 0.04.

Consider a plane electromagnetic wave with one component of magnetic field, H_z, and two components of electric field, E_ρ and E_ϕ, scattering on the inner electrode and the inhomogeneity of permittivity induced by it. Maxwell's equations allow us to derive the equation governing H_z as follows:

$$\rho^2 \frac{\partial^2 H_z}{\partial \rho^2} + \rho \left(1 - \rho \frac{\varepsilon'_{\text{eff}}(\rho)}{\varepsilon_{\text{eff}}(\rho)} \right) \frac{\partial H_z}{\partial \rho} + \frac{\partial^2 H_z}{\partial \phi^2} + k_0^2 \varepsilon_{\text{eff}}(\rho) \rho^2 H_z = 0, \quad (11)$$

where $\varepsilon'_{\text{eff}}(\rho) = d\varepsilon_{\text{eff}}(\rho)/d\rho$ is the derivative of the effective permittivity $\varepsilon_{\text{eff}}(\rho)$ and $k_0 = \omega/c$ is the free-space wavevector; ω is the frequency of the electromagnetic wave and c is the speed of light. The components of the electric field can be found as follows:

$$E_\rho = \frac{1}{ik_0\varepsilon_{\text{eff}}(\rho)}\frac{1}{\rho}\frac{\partial H_z}{\partial \phi}, \tag{12}$$

$$E_\phi = -\frac{1}{ik_0\varepsilon_{\text{eff}}(\rho)}\frac{\partial H_z}{\partial \rho}, \tag{13}$$

where i is the imaginary unit. Equations (11-13) must be completed by the boundary condition on the central electrode. Assuming that the electrode is a perfect electrical conductor, the boundary condition would state the vanishing of the tangential component of the electric field at the electrode surface, *i.e.*, $E_\phi|_{\rho=r_i} = 0$. However, in the case where the real part of the permittivity crosses zero, the electric field decreases exponentially in the region of negative permittivity. As a result, near the electrode surface, the electric field is very close to zero, and scattering from the electrode itself is negligibly small. In other words, the boundary condition is automatically satisfied in this case, because the electric field (including its tangential component) is already zero at the electrode surface.

After substituting $H_z(\rho) = \sum_{m=-\infty}^{\infty} H_z^{(m)}(\rho)\exp(im\phi)$, where m is an integer, and changing the variable as $\xi = k_0\rho$, Eq. (11) takes the form:

$$\frac{d^2H_z^{(m)}}{d\xi^2} + \left(\frac{1}{\xi} - \frac{\varepsilon'_{\text{eff}}(\xi)}{\varepsilon_{\text{eff}}(\xi)}\right)\frac{dH_z^{(m)}}{d\xi} + \left(\varepsilon_{\text{eff}}(\xi) - \frac{m^2}{\xi^2}\right)H_z^{(m)} = 0 \tag{14}$$

with the electric field components expressed as:

$$E_\rho^{(m)} = \frac{1}{\varepsilon_{\text{eff}}(\xi)}\frac{m}{\xi}H_z^{(m)}, \tag{15}$$

$$E_\phi^{(m)} = -\frac{1}{i\varepsilon_{\text{eff}}(\xi)}\frac{\partial H_z^{(m)}}{\partial \xi}. \tag{16}$$

Equation (14) does not allow for an analytical solution for an arbitrary $\varepsilon_{\text{eff}}(\xi)$. However, certain field characteristics can be found.

First, it can be seen that Eq. (14) has a singular point ξ_0, at which the effective permittivity becomes zero, $\varepsilon_{\text{eff}}(\xi_0) = 0$. The two linearly independent solutions of Eq. (14) in the vicinity of this point can be found as:

$$H_z^{(m)} \propto \sqrt{\frac{\varepsilon_{\text{eff}}(\xi)}{\xi}}M_{\kappa_m,1}\left(\frac{\kappa_m}{2}\frac{\xi-\xi_0}{\xi_0}\right), \sqrt{\frac{\varepsilon_{\text{eff}}(\xi)}{\xi}}W_{\kappa_m,1}\left(\frac{\kappa_m}{2}\frac{\xi-\xi_0}{\xi_0}\right), \tag{17}$$

where $\kappa_m = 2\sqrt{4m^2-1}$ and $M_{\kappa,\mu}(a)$ and $W_{\kappa,\mu}(a)$ represent the Whittaker functions of the arbitrary arguments κ, μ, and a. These solutions suggest that the magnetic field remains finite in the vicinity of the singular point. As a result, the radial component of the electric field is singular at ξ_0 for all harmonics except $m = 0$, since $E_\rho^{(m)}(\xi_0) \propto H_z^{(m)}(\xi_0)/\varepsilon_{\text{eff}}(\xi_0) \to \infty$. The behavior of the tangential component of the electric field turns out to be logarithmically divergent. Such a singularity is induced by a plasma-like resonance in the region where $\varepsilon_{\text{eff}} = 0$. Evidently, when the meta-atoms are lossy, *i.e.*, when the imaginary part of the effective permittivity is not zero, the electric field does not tend to infinity, but grows to some value defined by the losses. Consequently, when the imaginary part of the effective permittivity is small, *i.e.*, when $\text{Im}\varepsilon_{\text{eff}} \ll \text{Re}\varepsilon_{\text{eff}}$, the overall losses in the resonant region do not depend on the actual value of $\text{Im}\varepsilon_{\text{eff}}$. Indeed, the local electromagnetic loss density is proportional to $\text{Im}\varepsilon_{\text{eff}}|E|^2$, the maximum of $|E|^2$ is proportional to $(\text{Im}\varepsilon_{\text{eff}})^{-2}$, and the width of the resonance is proportional to $\text{Im}\varepsilon_{\text{eff}}$. Therefore, the total electromagnetic losses, defined by the integral of the loss density over the resonance region, do not depend on $\text{Im}\varepsilon_{\text{eff}}$. It should be emphasized that this resonance is a collective effect, which is not directly related to the plasmon resonance in a single particle. The considered resonance appears as a result of the crossing to zero of the effective permittivity and does not rely on any specific physical mechanism responsible for this crossing.

To analyze the scattering, it is useful to introduce the transverse impedance $Z_\perp = E_\perp/H_\perp \equiv E_\phi/H_z$. For each harmonic m, the impedance is governed by the following equation:

$$\frac{dZ_\perp^{(m)}}{d\xi} + \frac{1}{\xi}Z_\perp^{(m)} + i\varepsilon_{\text{eff}}(\xi)\left(Z_\perp^{(m)2} - Z_0^2(m,\xi)\right) = 0, \tag{18}$$

where $Z_0^2(m,\xi) = \varepsilon_{\text{eff}}^{-2}(\xi)\left(\varepsilon_{\text{eff}}(\xi) - m^2/\xi^2\right)$.

First, by knowing the solutions of Eq. (18), it is easy to find the scattering coefficients for each m and, therefore, the cross-section. The solutions of Eq. (18) can be found numerically, applying the boundary condition $Z_\perp^{(m)} = 0$ at the surface of the electrode, which corresponds to the vanishing of the tangential component of the electric field. Then, by fitting them to the analytical decomposition of the plane and scattered waves in the appropriate region, the reflection coefficients for each m can be calculated. Finally, by summing all the reflected waves, the total scattering cross-section can be found.

Second, Eq. (18) allows us to analyze the electromagnetic absorption in the resonant region near ξ_0 where $\text{Re}\varepsilon_{\text{eff}}(\xi_0) = 0$. The real part of the transverse impedance reveals a step behavior as a function of ξ in the vicinity of ξ_0. The magnitude of this step, $\text{Re}\Delta Z_\perp^{(m)}$, corresponds to the electromagnetic absorption density in a mode m. Since the real part of the impedance represents the energy flux density, the magnitude of its step corresponds to the decrease in the energy flux due to absorption, *i.e.*, electromagnetic losses. By analyzing Eq. (18), it can be concluded that $\text{Re}\Delta Z_\perp^{(m)} \propto m^2/\varepsilon'_{\text{eff}}(\xi_0)$ and does not depend on the imaginary part of the effective permittivity. Figure 3 shows the dependence of the total scattering cross-section and absorption cross-section on the applied voltage and the angular scattering patterns for different voltages.

In a particular realization of the proposed system, all the restrictions described above have to be taken into account. Thus, as a model system, let us introduce the following parameters.

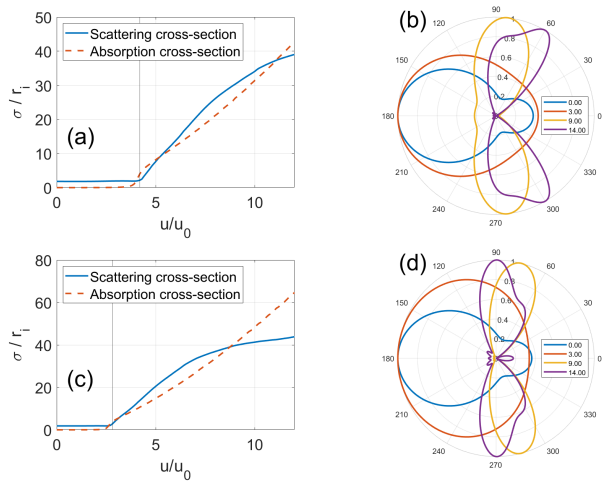

FIG. 3. Scattering and absorption cross-sections (a, c) and scattering diagrams (b, d) at different dimensionless voltages, u/u_0. The parameters are the same as in Fig. 2. The frequency was set to $\omega = 0.7\omega_p$ in (a, b) and $\omega = 0.64\omega_p$ in (c, d). The frequencies were chosen to be close to the plasmon resonance frequency, which is $3^{-1/2}\omega_p \approx 0.577\omega_p$.

The central metallic electrode has a radius of 1 μm. The meta-atoms are represented by doped semiconductor nanospheres of 10-nm radius with the plasma frequency of 100 THz. The meta-atoms are suspended in, *e.g.*, ethanol, which is transparent in the IR and has a refraction coefficient of ~ 1.4 in this frequency band. The unperturbed volume fraction was set to $\nu = 0.04$, which corresponds to the unperturbed meta-atom concentration of $\sim 10^{15}$ cm^{-3}. The characteristic voltage u_0 for such a system at room temperature is $u_0 \approx 39.5$ V. The system is illuminated by a plane TM-polarized electromagnetic wave at a frequency of $0.7\omega_p$, 70 THz. The corresponding wavelength in this medium is $\sim 3\mu$m, which is much larger than the meta-atom size. The specified parameters were used for the simulations presented in the following section.

III. SIMULATIONS

We performed full-wave simulations of the scattering of an electromagnetic wave on the permittivity distribution defined by Eqs. (2) and (9) using COMSOL Multiphysics software. For the simulations, the *Electromagnetic Waves, Frequency Domain* interface of the COMSOL RF Module was used. The permittivity distributions were calculated using custom software developed in Matlab and imported into COMSOL to set the permittivity distributions.

The color plots of the effective permittivity, electromagnetic loss, and radial and tangential field component distributions, as well as the absorption patterns for different applied potentials, are shown in Fig. 4.

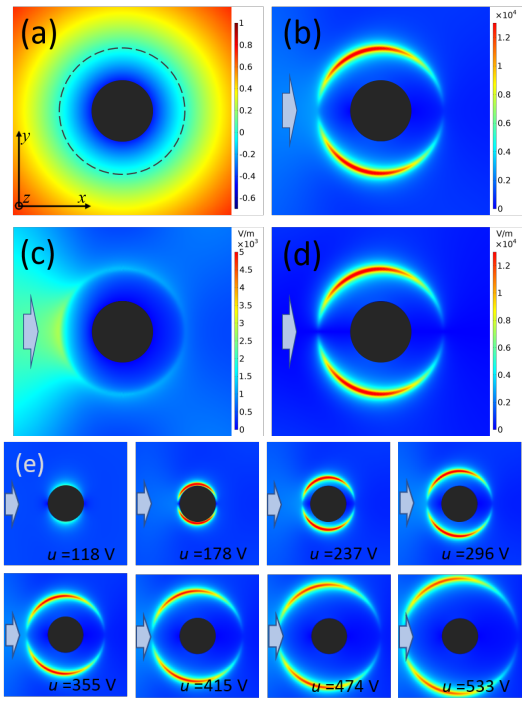

FIG. 4. Effective permittivity (a), electromagnetic absorption (b), tangential (c) and radial (d) components of the electric field, and electromagnetic absorption at different applied potentials (e). In (a), the dashed line represents the surface at which effective permittivity becomes zero, $\varepsilon_{\text{eff}} = 0$. In (a-d), the voltage is set to 335 V. In (e), the voltages are set to $118 - 533$ V ($u/u_0 = 3.0 - 13.5$), as noted in the lower right corner of each sub-image. The frequency is set to $\omega = 0.7\omega_p$. The radius of the central metallic electrode was set to 1 μm; the meta-atom radius was set to 10 nm; the plasma frequency of meta-atoms was set to 100 THz. The refraction index of the host liquid was set to 1.4. The unperturbed volume fraction of meta-atoms was set to $\nu = 0.04$. The temperature was set to 300 K. The arrows represent the direction of the wave propagation.

As can be seen, the resonant region appears at some threshold voltage and grows with the increase of the voltage. The radial distributions of the radial and tangential fields are shown in Fig. 5. It is noteworthy that the radial component of the electric field has a stronger resonant peak compared to the tangential component. Such a behavior is in accordance with the theoretical analysis: the radial component has a power divergence, while the tangential has a logarithmic divergence.

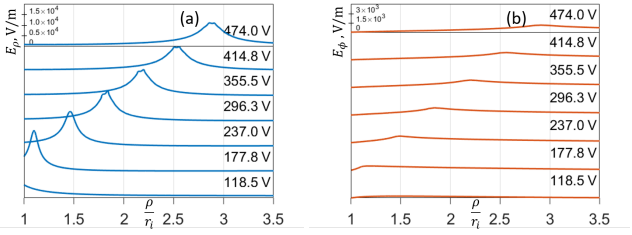

FIG. 5. Radial distribution of radial E_ρ (a) and tangential E_ϕ (b) components of the electric field at different voltages. The parameters are similar to those in Fig. 4.

Figure 6 shows the dependence of the electromagnetic field absorption cross-section σ in the resonant region as a function of the applied voltage for different values of the intrinsic meta-atom loss. As expected, when the intrinsic loss is not too high, the resonant absorption is almost independent of its value.

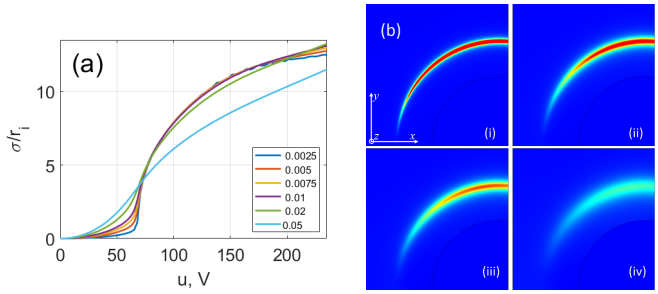

FIG. 6. Electromagnetic absorption cross-section as a function of voltage for different values of the normalized damping factor γ/ω_p (a), and color plots of the absorption in the plane transverse to the cylinder axis (b). For visibility, one quarter of the (circular) resonant region is shown. In (b), the normalized damping factor was set to 0.0025 (i), 0.005 (ii), 0.01 (iii), and 0.02 (iv). The frequency was set to $\omega = 0.64\omega_p$. Other parameters are similar to those in Fig. 4.

Figure 7 shows the energy flux in the scattering region. Evidently, the highest energy flux is in the resonance region; its direction is along the surface, where $\mathrm{Re}\varepsilon_{\mathrm{eff}} = 0$. Such a behavior is an indication of the excitation of the surface wave at the interface between the regions with $\mathrm{Re}\varepsilon_{\mathrm{eff}} > 0$ and $\mathrm{Re}\varepsilon_{\mathrm{eff}} < 0$.

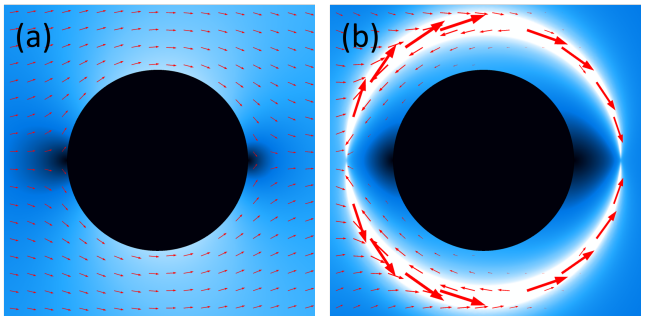

FIG. 7. Energy flux (Poynting vector field) in the scattering region. The voltage was set to 0 V (below the threshold) (a) and 158 V (above the threshold) (b). The other parameters are similar to those in Fig. 4. The arrows represent the Poynting vector. The lengths of the arrows are proportional to the logarithm of the Poynting vector moduli.

Videos of plane wave scattering on the liquid MM distributions (Visualizations 1-3) and animation of the influence of the real-time voltage change on the absorption (Visualization 4) are available in the supporting materials.

IV. DISCUSSION

The considered scattering problem may be of interest in several aspects. In particular, the interaction between the electromagnetic wave and the system is controlled by a simple variation of the electric potential of the immersed electrode. Below some threshold value, the scattering almost does not depend on the voltage, being just the scattering off the central cylindrical electrode. However, when the voltage exceeds this threshold, the scattering characteristics change drastically.

First, the total scattering cross-section starts to grow with the increase of the voltage up to a certain maximum. This can be partially attributed to the growth of the scattering region. Indeed, the scatterer is no longer the central electrode, but the surface surrounding the volume whose meta-atom concentration is high enough to make the permittivity negative. However, because of the resonant nature of the scattering, the cross-section grows faster than the actual scatterer size. Namely, below the threshold, the cross-section roughly equals the diameter of the central electrode. On the other hand, above the threshold, the scattering cross-section becomes significantly larger than the scattering region diameter. For instance, at the frequency of $0.7\omega_p$, the diameter of the scattering area reaches $3.36r_i$, while the total cross-section reaches $40r_i$; at the frequency of $0.64\omega_p$, the diameter of the scattering area reaches $5.1r_i$, and the total cross-section grows as high as $50r_i$.

At the same time, although the total cross-section increases when the voltage threshold is reached, the backscattering is suppressed. As can be seen in Figs. 3 (b) and (d), while at zero voltage the preferential scattering direction is backwards (with respect to the wave propagation), with the increase of the voltage the backscattering is reduced. Moreover, for certain parameter combinations,*e.g.* at the frequency of $0.7\omega_p$ and the dimensionless voltage of $u/u_0 = 9$, or at the frequency of $0.64\omega_p$ and the dimensionless voltage of $u/u_0 = 14$, the backscattering is almost entirely eliminated.

Another feature of the considered scattering mechanism is the associated resonant absorption. It takes place in a thin layer nearby the surface, at which the real part of the effective permittivity is zero. A similar effect has been studied in inhomogeneous plasma [38]. Resonant absorption appears at the voltage threshold, similarly to resonant scattering. However, while the scattering cross-section is a continuous function of the voltage, the absorption presents a discontinuous step at the threshold. It can be understood as the immediate appearance of finite absorption as soon as the real part of the effective permittivity crosses zero. Since the absorption takes place in a very narrow region, a very small increase in voltage is needed for the resonant region to fit between the $\mathrm{Re}\varepsilon_{\mathrm{eff}} = 0$ surface and the surface of the central electrode. The width of the resonant region is governed by the damping factor of the meta-atom material. Evidently, the larger the damping is, the wider becomes the resonant region. At the same time, the maximum field amplitude and, therefore, the maximum loss depend inversely on damping: the larger the damping, the smaller the field maximum. These two effects compensate each other keeping the total loss constant as long as the damping is not too large. This can be seen in Fig. 6. Indeed, in Fig. 6 (a), the energy loss plots follow almost the same line for different values of damping, confirming the suggested property. In Fig. 6 (b), the variations of the loss region width and loss intensity depending on the damping factor are clearly visible.

The narrowness of the resonant region can be exploited for local electromagnetic heating. Clearly, as a major part of the electromagnetic power is absorbed in a thin layer near $\mathrm{Re}\varepsilon_{\mathrm{eff}} = 0$, this layer inevitably becomes a heat source. Moreover, because of the independence of the losses from the damping factor, the heat generation in the layer does not depend on the damping factor either, and, more broadly, on the nature of the loss in the meta-atoms.

Finally, the region limited by the surface $\mathrm{Re}\varepsilon_{\mathrm{eff}} = 0$, including the central electrode itself, turns out to be effectively shielded. Namely, the electromagnetic wave can hardly penetrate the region such that $\mathrm{Re}\varepsilon_{\mathrm{eff}} < 0$, which makes it isolated from the electromagnetic radiation.

It should be noted that all of the listed effects can be controlled by the application of a voltage to the central electrode. By varying the voltage, the resonant absorption can be turned off or on, its intensity can be altered; the backscattering can be minimized, the total scattering can be manipulated; the central region can be shielded.

As was already mentioned, the proposed system is scalable in the sense that as long as the homogenization applicability conditions are satisfied, the parameters of the system, such as the meta-atom size and the negative polarizability mechanism, the electromagnetic wave frequency, and the overall size of the system, may vary significantly. In the previous sections, we have considered the system designed for 70-THz infrared radiation. At the same time, the system can be scaled for either higher or lower frequencies by varying the sizes and choosing the meta-atom materials. For instance, the meta-atoms can be made of highly doped GaAs with the dopant concentration of 6×10^{16} cm^{-3} and the corresponding plasma frequency of 14.9 THz. As a result, a suspension of such nanoparticles with the radius of 600 nm and the volume fraction of 0.08 placed in a 0.5-mm-diameter transparent cylindrical vessel with a 6-μm-thick copper electrode immersed in its center would provide an alternative realization of the proposed system. The corresponding electromagnetic frequency band, within which the effects described above would be prominent, would lie between 6.34 and 14.9 THz. Conversely, the system can be scaled for higher-frequency band by choosing metal particles of a few nanometers in diameter as meta-atoms and a wire of 100 nanometers in diameter as the electrode. For instance, for Ag nanoparticles with the plasma frequency of 2200 THz, the applicable frequency band would lie between 1500 and 2000 THz.

One possible realization of a device based on the effect described above can be an array of cylindrical cells, each of which is represented by the proposed system. By manipulating the voltages applied to each cell, one could control the transparency, absorption, and backscattering of such a panel. Another possible application is mode manipulation in a waveguide or a resonator. Again, by simply applying the voltage, the Q-factor can be drastically decreased, thus providing controlled damping.

V. CONCLUSION

We have considered the scattering of a plane electromagnetic wave on the cylindrically symmetric inhomogeneous distribution of a liquid MM induced by a static electric field, which can be generated by applying an electric potential to an electrode immersed in the liquid MM. We have shown that by changing the voltage, it is possible to manipulate the scattering of this wave in different ways. For instance, the scattering cross-section can be varied over a wide range. By tuning the voltage, backscattering can be suppressed. In addition, in the scattering region, resonant absorption enhanced by the excitation of a surface wave takes place. The proposed controlled scattering mechanism benefits from the particular simplicity of all its constituents. For instance, the meta-atoms can be any spherical particles that can provide negative polarizability at a certain frequency, *i.e.*, metallic or high-index dielectric spheres. The host liquid and the outer boundaries just have to be transparent for the electromagnetic wave at that frequency. Thus, a realization of the proposed mechanism may be used for controllable shielding, controllable backscattering suppression, or manipulation with scattering.

Funding. This study was supported by the French PIA project "Lorraine Université d'Excellence", reference ANR-15-IDEX-04-LUE and TALiSMAN project, funded by ERDF (2019-000214).

Disclosures. The authors declare no conflicts of interest.

Data availability. No data were generated or analyzed in the presented research.

Supplemental document. See Visualizations 1-4 for supporting content.

* alexander.zharov@univ-lorraine.fr
† alain.celzard@univ-lorraine.fr

[1] D. R. Smith, W. J. Padilla, D. C. Vier, S. C. Nemat-Nasser, and S. Schultz, "Composite medium with simultaneously negative permeability and permittivity," Phys. Rev. Lett. **84**, 4184-4187 (2000).

[2] R. A. Shelby, D. R. Smith, and S. Schultz, "Experimental verification of a negative index of refraction," Science **292**, 77-79 (2001).

[3] S. Linden, C. Enkrich, M. Wegener, T. Zhou, T. Kochny, and C. M. Soukoulis, "Magnetic response of metamaterials at 100 terahertz," Science **306**, 1351-1353 (2004).

[4] S. Zhang, W. Fan, B. K. Minhas, A. Frauenglass, K. J. Malloy, and S. R. J. Brueck, "Midinfrared resonant magnetic nanostructures exhibiting a negative permeability," Phys. Rev. Lett. **94**, 037402 (2005).

[5] H. J. Lezec, J. A. Dionne, and H. A. Atwater, "Negative refraction at visible frequencies," Science **316**, 430-432 (2007).

[6] A. Minovich, J. Farnell, D. N. Neshev, I. McKervacher, F. Karouta, J. Tian, D. A. Powell, I. V. Shadrivov, H. H. Tan, C. Jagadish, and Y. S. Kivshar, "Liquid crystal based nonlinear fishnet metamaterials," Appl. Phys. Lett. **100**, 121113 (2012).

[7] A. A. Zharov, I. V. Shadrivov, and Y. S. Kivshar, "Nonlinear properties of left-handed metamaterials," Phys. Rev. Lett. **91**,

037401 (2003).
[8] M. Lapine, I. V. Shadrivov, D. A. Powell, and Y. S. Kivshar, "Metamaterials with conformational nonlinearity," Sci. Rep. **1**, 138 (2011).
[9] M. Lapine, I. V. Shadrivov, D. A. Powell, and Y. S. Kivshar, "Magnetoelastic metamaterials," Nat. Mater. **11**, 30-33 (2012).
[10] A. P. Slobozhanyuk, M. Lapine, D. A. Powell, I. V. Shadrivov, Y. S. Kivshar, R. C. McPherdan, and P. A. Belov, "Flexible helices for nonlinear metamaterials," Adv. Mater. **25**, 3409-3412 (2013).
[11] D. Liu, Y.-L. Hong, R.-H. Fan, H. Jing, R.-W. Peng, Y. Lai, X.-R. Huang, C. Sun, and M. Wang, "Bendable disordered metamaterials for broadband terahertz invisibility," Opt. Express **28**, 3552-3560 (2020).
[12] A. K. Boddeti, A. Alabassi, V. Aggarwal, and Z. Jacob, "Spectral domain inverse design for accelerating nanocomposite metamaterials discovery," Opt. Mater. Express **9**, 4765-4771 (2019).
[13] W. L. Bames, A. Dereux, and A. Ebbensen, "Surface plasmon subwavelength optics," Nature **424**, 824-830 (2003).
[14] V. M. Shalaev and S. Kawata, "Nanophotonics with Surface Plasmons" (Elsevier Science, 2007).
[15] M. A. Noginov, Y. A. Barnakov, G. Zhu, T. Tumkur, H. Li, and E. E. Narimanov, "Bulk photonic metamaterial with hyperbolic dispersion," Appl. Phys. Lett. **94**, 151105 (2009).
[16] Y. Guo, W. Newman, C. L. Cortes, and Z. Jacob, "Applications of hyperbolic metamaterial substrates," Adv. Opt. Electron. **2012**, 452502 (2012).
[17] A. Poddubny, I. V. Iorsh, P. A. Belov, and Y. S. Kivshar, "Hyperbolic metamaterials," Nat. Photonics **7**, 948-957 (2013).
[18] D. Schurig, J. J. Mock, B. J. Justice, S. A. Cummer, J. B. Pendry, A. F. Starr, and D. R. Smith, "Metamaterial electromagnetic cloak at microwave frequencies," Science **314**, 977-980 (2006).
[19] B. Edwards, A. Alu, M. G. Silveirinha, and N. Engheta, "Experimental verification of plasmonic cloaking at microwave frequencies with metamaterials," Phys. Rev. Lett. **103**, 153901 (2009).
[20] J. B. Pendry, "Negative refraction makes a perfect lens," Phys. Rev. Lett. **85**, 3966 (2000).
[21] P. A. Belov, Y. Hao, and S. Sudhakaran, "Subwavelength microwave imaging using an array of parallel conducting wires as a lens," Phys. Rev. B **73**, 033108 (2006).
[22] J. B. Pendry, D. Schurig, and D. R. Smith, "Controlling electromagnetic fields," Science **312**, 1780-1782 (2006).
[23] U. Leonhardt, "Optical conformal mapping," Science **312**, 1777-1780 (2006).
[24] Y. Tang and A. E. Cohen, "Optical chirality and its interaction with matter," Phys. Rev. Lett. **104**, 163901 (2010).
[25] E. Plum, V. A. Fedotov, and N. I. Zheludev, "Optical activity in extrinsiccally chiral metamaterial," Appl. Phys. Lett. **93**, 191911 (2008).
[26] W. Zhang, Q. Song, W. Zhu, Z. Shen, P. Chong, D. P. Tsai, C. Qiu, and A. Q. Liu, "Metafluidic metamaterial: a review," Advances in Physics: X, **3:1** (2018).
[27] Y. A. Urzhumov, G. Shvets, J. A. Fan, F. Capasso, D. Brandl, and P. Nordlander, "Plasmonic nanoclusters: a path towards negative-index metafluids," Opt. Express **15**, 14129-14145 (2007).
[28] M. Fruhnert, S. Muhlig, F. Lederer, and C. Rockstuhl, "Towards negative index self-assembled metamaterials," Phys. Rev. B **89**, 075408 (2014).
[29] A. B. Golovin, O. D. Lavrentovich, "Electrically reconfigurable optical metamaterial based on colloidal dispersion of metal nano-rods in dielectric fluid," Appl. Phys. Lett. **95**, 254104 (2009).
[30] Q. Liu, Y. Cui, D. Gardner, X. Li, S. He, I. I. Smalyukh, "Self-Alignment of Plasmonic Gold Nanorods in Reconfigurable Anisotropic Fluids for Tunable Bulk Metamaterial Applications," Nano Lett. **10**, 1347 (2010).
[31] A. A. Zharov, A. A. Zharov, Jr., and N. A. Zharova, "Liquid metacrystals," J. Opt. Soc. Am. B **31**, 559-564 (2014).
[32] A. A. Zharov, A. A. Zharov, Jr., and N. A. Zharova, "Spontaneous reorientations of meta-atoms and electromagnetic spatial solitons in a liquid metacrystal," Phys. Rev. E **90**, 023207 (2014).
[33] M. Liu, K. Fan, W. Padilla, X. Zhang, and I. V. Shadrivov, "Tunable meta-liquid crystals," Adv. Mater. **28**, 1553-1558 (2016).
[34] A. Zharov, Z. Viskadourakis, G. Kenanakis, V. Fierro, and A. Celzard, "Control of Light Transmission in a Plasmonic Liquid Metacrystal," Nanomaterials **11**, 346 (2021).
[35] A. Zharov, V. Fierro, and A. Celzard, "All-dielectric bulk isotropic double-negative metamaterials," J. Opt. Soc. Am. B **38**, 159-166 (2021).
[36] E. A. Gibson, M. Pennybacker, A. I. Maimistov, I. R. Gabitov, and N. M. Litchinitser, "Resonant absorption in transition metamaterials: parametric study," J. Opt. **13**, 024013 (2010).
[37] E. A. Gibson, I. R. Gabitov, A. I. Maimistov, and N. M. Litchinitser, "Transition metamaterials with spatially separated zeros," Opt. Lett. **36**, 3624-3626 (2011).
[38] N. G. Denisov, "On a singularity of the field of an electromagnetic wave propagated in an inhomogeneous plasma," Sov. Phys. JETP **4**, 544 (1957).
[39] A. Malasi, R. Kalyanaraman, and H. Garcia, "From Mie to Fresnel through effective medium approximation with multipole contributions," J. Opt.
[40] C. M. Butler, "Capacitance of a finite-length conducting cylindrical tube," J. Appl. Phys. **51**, 5607 (1980).